nature nanotechnology

LETTERS

PUBLISHED ONLINE: 25 MARCH 2012 | DOI: 10.1038/NNANO.2012.34

Real-time single-molecule imaging of quantum interference

Thomas Juffmann[1], Adriana Milic[1], Michael Müllneritsch[1], Peter Asenbaum[1], Alexander Tsukernik[2], Jens Tüxen[3], Marcel Mayor[3,4], Ori Cheshnovsky[2,5] and Markus Arndt[1]*

The observation of interference patterns in double-slit experiments with massive particles is generally regarded as the ultimate demonstration of the quantum nature of these objects. Such matter–wave interference has been observed for electrons[1], neutrons[2], atoms[3,4] and molecules[5–7] and, in contrast to classical physics, quantum interference can be observed when single particles arrive at the detector one by one. The build-up of such patterns in experiments with electrons has been described as the "most beautiful experiment in physics"[8–11]. Here, we show how a combination of nanofabrication and nano-imaging allows us to record the full two-dimensional build-up of quantum interference patterns in real time for phthalocyanine molecules and for derivatives of phthalocyanine molecules, which have masses of 514 AMU and 1,298 AMU respectively. A laser-controlled micro-evaporation source was used to produce a beam of molecules with the required intensity and coherence, and the gratings were machined in 10-nm-thick silicon nitride membranes to reduce the effect of van der Waals forces. Wide-field fluorescence microscopy detected the position of each molecule with an accuracy of 10 nm and revealed the build-up of a deterministic ensemble interference pattern from single molecules that arrived stochastically at the detector. In addition to providing this particularly clear demonstration of wave–particle duality, our approach could also be used to study larger molecules and explore the boundary between quantum and classical physics.

When Richard Feynman described the double-slit experiment with electrons as being 'at the heart of quantum physics'[12] he was emphasizing how the fundamentally non-classical nature of the superposition principle allows the quantum wavefunction associated with a massive object to be widely delocalized, while the object itself is always observed as a well-localized particle. Recent experiments have focused this discussion by demonstrating the stochastic build-up of interference patterns[11,13], by implementing double-slit diffraction in the time domain[14,15] (including down to the attosecond level[16]), and by identifying a single molecule as the smallest double-slit for electron interference[17,18] that enables fundamental studies of decoherence[19]. The extension of this work[20] to large molecules requires a sufficiently intense and coherent beam of slow and neutral molecules, a nanoscale diffraction grating, and a detector that offers a spatial accuracy of a few nanometres and a molecule-specific detection efficiency of close to 100%. We achieve that in this work with a combination of micro-evaporation, nanofabrication and nano-imaging.

Our experimental set-up comprises three sections: beam preparation, coherent manipulation and detection (Fig. 1). The molecules need to be prepared such that each one interferes with itself, and all lead to similar interference patterns on the screen. Because the transverse and longitudinal coherence functions are determined by the Fourier transforms of the source spatial extension and velocity distribution[21], we require a good collimation and velocity selection. Under 'far-field' conditions we can approximate the molecular wavefunctions as plane waves, and the angle θ_n of the nth order diffraction peak is given by the equation $\sin\theta_n = n\Lambda/d$, where $\Lambda = h/mv$ is the de Broglie wavelength, h is Planck's constant, m is the particle mass, v is the velocity, and d is the period of the diffraction grating. Massive particles therefore need to be slow to achieve sizable diffraction angles. Although deceleration techniques have been advanced for molecules even as complex as benzonitrile[22], effusive beams (Fig. 1b) are still well suited for preparing slow beams of particles a hundred times more massive than that[23,24].

For thermolabile organic molecules, which may decompose when heated to their evaporation temperature, we use a laser micro-source (Fig. 1a), which reduces the heat load to a minimum. A blue diode laser is focused onto a thin layer of molecules deposited on the inside of the entrance vacuum window W_1, which can be moved by a motorized translation stage. Although high temperatures can be reached locally, this affects only the particles within the focus area. In comparison to a Knudsen cell, the heat load to the sample is therefore reduced by two to three orders of magnitude (to several 10 mW). Spectral coherence is achieved by sorting the arriving molecules according to their longitudinal velocity and their respective freefall height in the Earth's gravitational field[25].

The collimation slit S defines the spatial coherence of the molecular beam. The slit and the grating width further downstream narrow the beam divergence to less than the diffraction angle. The grating is machined into a thin SiN_x membrane and has a period of $d = 100$ nm. To minimize the dispersive van der Waals interaction between the molecules and the grating wall we reduce the grating thickness from 160 nm (as in earlier diffraction experiments[5,20]) to as little as 10 nm in our present set-up. This is important for the manipulation of complex molecules, which may exhibit high polarizabilities, permanent and even thermally induced electric dipole moments[26,27]. Each individually diffracted molecule finally arrives at the 170-μm-thin quartz plate W_2, which seals the detector vacuum chamber against ambient air. The gradual emergence of the quantum interference pattern is then observed by means of wide-field fluorescence microscopy of W_2.

Imaging of single molecules in the condensed phase began about two decades ago[28], and various methods for subwavelength optical imaging have been developed since[29]. Here, we make use of a scheme that is similar to single-molecule high-resolution imaging

[1]Vienna Center of Quantum Science and Technology, Faculty of Physics, University of Vienna, Boltzmanngasse 5, 1090 Vienna, Austria, [2]The Center for Nanoscience and Nanotechnology, Tel Aviv University, 69978 Tel Aviv, Israel, [3]Department of Chemistry, University of Basel, St. Johannsring 19, 4056 Basel, Switzerland, [4]Karlsruhe Institute of Technology, Institute for Nanotechnology, PO Box 3640, 76021 Karlsruhe, Germany, [5]School of Chemistry, The Raymond and Beverly Sackler faculty of exact sciences, Tel Aviv University, 69978 Tel Aviv, Israel. *e-mail: markus.arndt@univie.ac.at

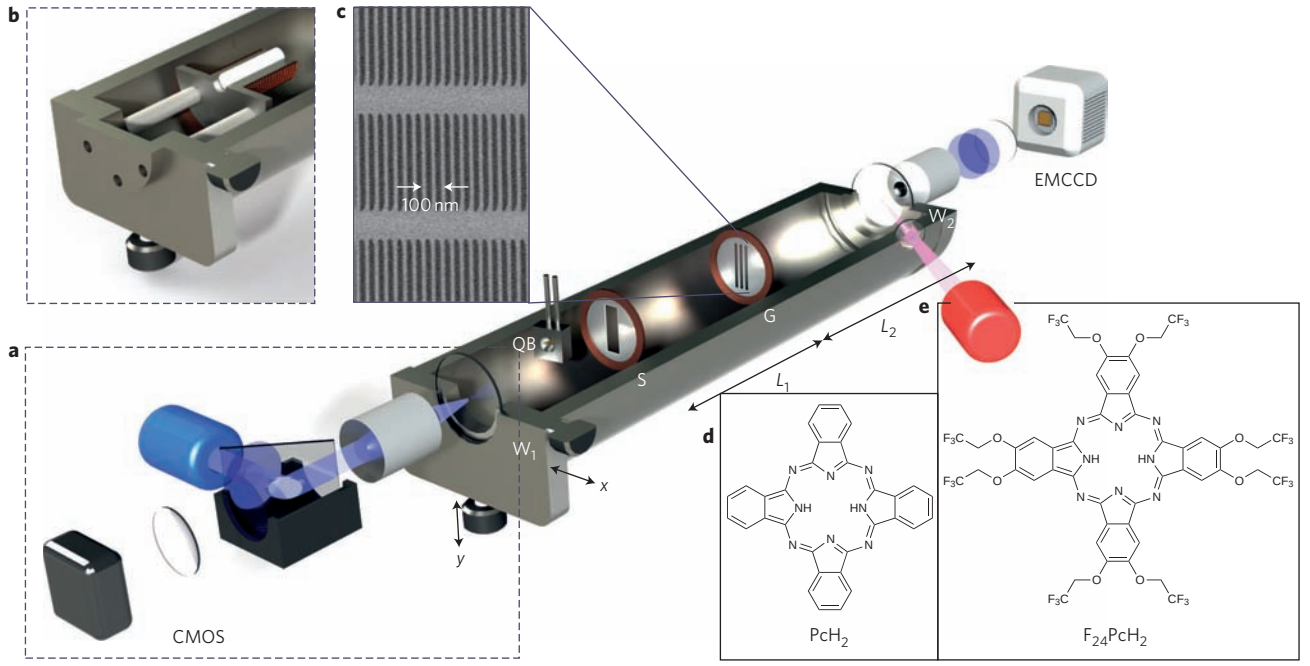

Figure 1 | Set-up for laser-evaporation, diffraction and nano-imaging of complex molecules. a, Thermolabile molecules are ejected by laser micro-evaporation. A blue diode laser (445 nm, 50 mW) is focused onto window W_1 to evaporate the molecules coated on its inner surface. A CMOS camera and a quartz balance (QB) monitor the evaporation area and the molecular flux. **b**, Stable molecules can be evaporated in a Knudsen cell. The collimation slit S defines the beam coherence. The molecular beam divergence is further narrowed by the width of the diffraction grating G. **c**, Electron micrograph showing that the grating is nanomachined into a 10-nm-thin SiN_x membrane with a period of $d = 100$ nm. The vacuum system is evacuated to 1×10^{-8} mbar. Molecules on quartz window W_2 are excited by a red diode laser (661 nm). High-resolution optics collects, filters and images the light onto an EMCCD camera. **d**,**e**, The molecules for this study: phthalocyanine PcH_2 ($C_{32}H_{18}N_8$, mass $m = 514$ AMU, number of atoms $N = 58$, **d**) and its derivative $F_{24}PcH_2$ ($C_{48}H_{26}F_{24}N_8O_8$, $m = 1{,}298$ AMU, $N = 114$, **e**). The mass, atomic number and internal complexity of $F_{24}PcH_2$ are approximately twice those of PcH_2.

with photo-bleaching (SHRIMP)[30]. Even if the pointspread function of an optical emitter is bound to Abbé's diffraction limit, it is still possible to determine its barycentre with nanometre accuracy, if the signal-to-noise ratio is high enough and as long as the point-spread functions of neighbouring molecules do not overlap.

The phthalocyanine molecule PcH_2 (Fig. 1d) and its derivative $F_{24}PcH_2$ (Fig. 1e) were selected because they are stable molecules and efficient dyes, even in vacuum. The molecular sample on W_2 was illuminated under a shallow angle so that the excitation laser did not enter the imaging optics. Fluorescence was collected by a microscope objective, filtered, and imaged onto the single-photon-sensitive electron-multiplying charge-coupled device (EMCCD) camera. (See Supplementary Table S3 for full details of the imaging optics.)

Figure 2 shows a typical fluorescence image of surface-deposited phthalocyanine molecules. We detect $\sim 1 \times 10^5$ fluorescence photons per molecule before abrupt bleaching or desorption is observed from one frame to the next, in support of the claim that we monitor single molecules and not aggregates. By fitting a two-dimensional Gaussian to each molecular image we can determine its position with an accuracy of 10 nm. This would even fulfil the detector requirements of matter–wave near-field interferometry[31].

The high detection efficiency exceeds that of electron-impact quadrupole mass spectrometry by more than a factor of 10^4. This large gain allows us, for the first time, to optically visualize the real-time build-up of a two-dimensional quantum interference pattern from stochastically arriving single molecules, as shown in Fig. 3. This series was recorded with an effusive source (Fig. 1b) heated to 750 K. A typical velocity of 150 m s^{-1} then corresponds to a de Broglie wavelength of $\Lambda_{dB} = 5.2$ pm. The actual velocity distribution is reconstructed from the molecular height distribution on the detection screen and turns out to be slightly faster and narrower than thermal. The pictures represent a balance of the continuous accumulation of molecules and intermittent bleaching by the imaging laser (3 s per frame for Fig. 3a–d). Figure 3 shows the

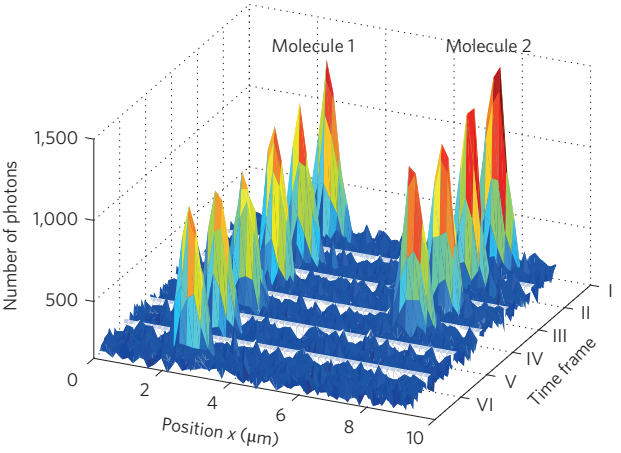

Figure 2 | Single-molecule imaging of PcH_2 with subwavelength accuracy. Plots show photon numbers at various position at six different time points (starting at the back), as extracted from the frames of a movie recorded with an EMCCD camera. Two molecules are localized on the quartz surface next to one another. After frame IV, molecule 2 either bleaches or desorbs again. Our experiments indicate that bleaching typically occurs after the detection of $\sim 1 \times 10^5$ photons. We detect each molecule with a signal-to-noise ratio of ~20, which enables us to determine the barycentre of their pointspread function with an accuracy of ~10 nm. Most molecules remain immobilized on the nanoscale and the interference pattern persists even over days.

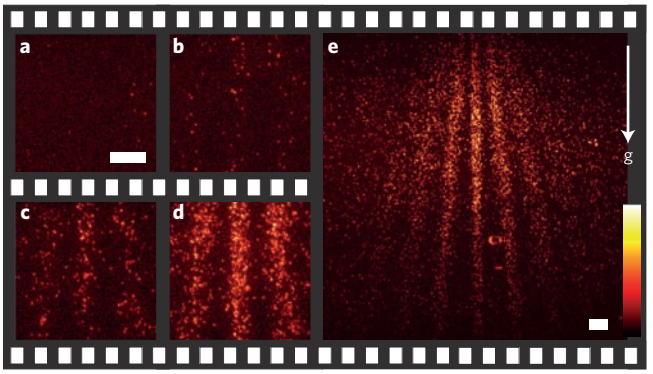

Figure 3 | Build-up of quantum interference. a–e, Selected frames from a false-colour movie recorded with an EMCCD camera showing the build-up of the quantum interference pattern for PcH_2 molecules. Images were recorded before deposition of the molecules (**a**) and 2 min (**b**), 20 min (**c**), 40 min (**d**) and 90 min (**e**) after deposition. Scale bars, 20 μm (**a–e**). The colour bar ranges from −5 to 120 photons in **a–d** and from −20 to 650 photons in **e**. **a–d** are taken from Supplementary Movie 1, and the wide-field view in **e** is taken with the same objective as Supplementary Movie 2. The movie frame rate was 0.1 Hz for the first 20 min (**a–c**). Thereafter it was reduced to 0.05 Hz to allow for another dynamic equilibrium of bleaching and the arrival of fresh molecules. Collimation slit S (Fig. 1) was cut into a 50-nm-thick SiN membrane and had dimensions of 1 μm (width) and 100 μm (height). Diffraction grating G was cut into a 10-nm-thick SiN membrane (width, 5 μm; height, 100 μm), with period $d = 100$ nm. Width of the individual slits: $s = 50$ nm. $L_1 = 702$ mm, $L_2 = 564$ mm. The arrow pointing downwards indicates the direction of the gravitational acceleration g.

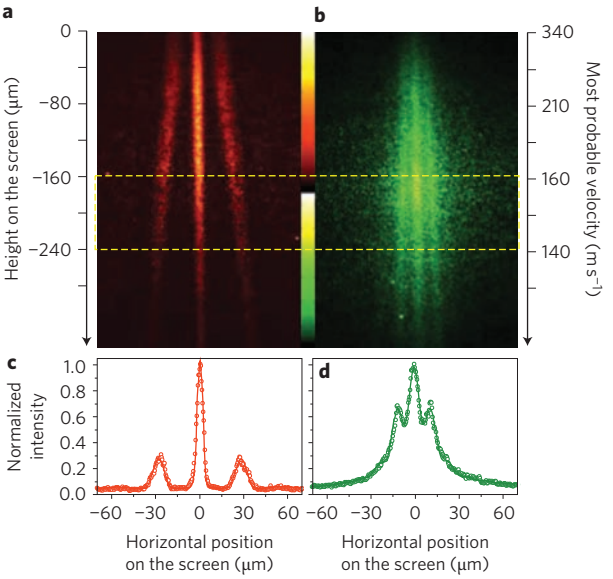

Figure 4 | Comparison of interference patterns for PcH_2 and $F_{24}PcH_2$. **a**,**b**, False-colour fluorescence images of the quantum interference patterns of PcH_2 (**a**) and $F_{24}PcH_2$ (**b**). We can deduce both the mass and the velocity of the molecules from these images, because diffraction spreads out the molecular beam in the horizontal direction, and the effects of gravity mean that the height h on the screen (left axes) depends on the velocity v of the molecule (right axes). The colour bar ranges from −20 to 400 photons in **a**, and from −20 to 600 photons in **b**. The true fluorescence of both molecules starts at wavelengths above 700 nm. **c**,**d**, One-dimensional diffraction curves obtained by integrating the fluorescence images in **a** and **b** between $h = -160$ μm and $h = -240$ μm (dashed yellow lines in **a** and **b**), which corresponds to velocity spread $\Delta v/v = 0.27$. All imaging settings are specified in Supplementary Table S1. Collimation slit S (Fig. 1) was 3 μm wide (defined by a pair of steel razor blades with 300 nm edge width). Diffraction grating G was cut into a 10-nm-thick SiN membrane and had dimensions of 3 μm (width) and 100 μm (height), with period $d = 100$ nm (width of individual slits $s = 75$ nm). $L_1 = 566$ mm, $L_2 = 564$ mm.

influence of the van der Waals force quite clearly. The high fringe visibility up to the fourth interference order can only be explained by an effective slit narrowing[32] by a factor of about two due to the molecule–wall interaction, even for gratings as thin as 100 atomic monolayers. The relative importance of the molecule–wall interaction is discussed in the Methods and Supplementary Fig. S2.

The high sensitivity of fluorescence detection now also allows us to extend far-field diffraction to more complex molecules. In Fig. 4 we compare specifically the interference pattern of the fluoroalkylated phthalocyanine $F_{24}PcH_2$ with that of PcH_2, both starting from the new laser micro-evaporation source (Fig. 1a), which allows us to record the interference patterns with a material consumption 100 times smaller than when using a Knudsen cell.

To account for the higher polarizability of $F_{24}PcH_2$, this experiment was performed with wider slits (75 nm) than those used for Fig. 3 ($s = 50$ nm). Again, we see clear quantum interference. We retrieve one-dimensional projections from the two-dimensional diffraction patterns by vertically integrating over a part of the velocity distribution (Fig. 4c,d). The solid lines in these diagrams represent the textbook-like diffraction of plane waves at a grating. They also include an incoherent average over the known source extension as well as over the detected velocity range. We find agreement between the numerical model and our experiment if we fit a van der Waals constant of $C_3 = 16$ meV nm^3 for PcH_2 and $C_3 = 98$ meV nm^3 for $F_{24}PcH_2$ in the interaction with the SiN_x walls. Details of the modelling are available in the Methods and the Supplementary Information.

The uncertainty in this fit is estimated to be ∼50%. Precision measurements of C_3 will become possible in the future with a more accurate determination of the open slit width across the entire grating, better velocity selection, systematic variation of the grating thickness, and a more rigorous theoretical description of the molecule–wall interaction. To obtain the numerical fit of Fig. 4d it was necessary to convolute the calculated interference pattern with a Gaussian with a standard deviation of 3 μm. This smearing may be attributed either to surface diffusion or to a low contribution of fragmented molecules within the molecular beam. Diffusion would in fact be consistent with the design specifications of this molecule: $F_{24}PcH_2$ is fluorinated to reduce its binding to the surroundings, to facilitate evaporation. Note that in contrast to Fig. 3 the patterns of Fig. 4 show high contrast only to the first diffraction order. This is related to the larger grating slit width used in this experiment.

Compared to our previous molecular far-field experiments[6], we have improved the source economy by a factor of 1,000, reduced the grating thickness (and the corresponding van der Waals phase shift) by a factor of 16, and increased the detection efficiency to the level of single molecules. Fluorescence imaging with nanometre accuracy is orders of magnitude more sensitive than the ionization methods used in previous work, and it should be possible to detect many natural and functionalized organic molecules, and also quantum dots, with this method. Scanning tunnelling microscopy has been used for single-molecule interference imaging[33], but our approach offers recording speeds that can be up to 1,000 times faster over an imaging area that is 10^5 times larger. Although the effects of the van der Waals force are still evident for membranes as thin as 10 nm, it should be possible to reduce or even eliminate these effects in future experiments by using gratings made of double-layer graphene or made of light[34].

The diffraction of single molecules at a grating is an unambiguous demonstration of the wave–particle duality of quantum physics[35,36]. It is only explicable in quantum terms, independent

of the absolute value of the interference contrast. In contrast to photons and electrons, which are irretrievably lost in the detection process, fluorescent molecules stay in place to provide clear and tangible evidence of the quantum behaviour of large molecules.

Methods

Molecular synthesis and sample preparation. The three-step synthesis of $F_{24}PcH_2$ comprises the formation of a fluorinated phthalonitrile followed by the assembly of a fluorous zinc phthalocyanine derivative and a final demetallation step[37] (see Supplementary Methods for synthetic protocols and analytical data). A solution (PcH_2)/suspension ($F_{24}PcH_2$) of molecules in acetone was smeared onto the BK7 entrance window to form a thin layer. Inhomogeneities in the sample thickness may occur but do not influence the final diffraction pattern. We observed some liquefaction during the micro-evaporation, which also homogenized the sample.

Fabrication of the nanogratings. The SiN_x gratings were produced by focused ion beam (FIB) milling into a 10-nm-thin membrane (from TEMWINDOWS.com). The FIB milling was carried out in the ionLiNE system (from RAITH GmbH) using gallium ions at $E = 35$ keV and with currents ranging from 1 pA to 7 pA. The gratings have a period of 100 nm and opening widths of 50 nm (Fig. 4a) and 75 nm (Fig. 4b).

Cleaning the quartz window. *In situ* plasma cleaning was used to clean the surface of the quartz window. Outside: air at atmospheric pressure. Inside: nitrogen at 1 mbar. Discharge: a.c. voltage of 1.5 kV and 10 kHz, with a 0.5 mm electrode at a distance of 0.5 mm from the window. The grounded vacuum chamber served as the counter-electrode.

Numerical modelling of the diffraction images. We fit our data using diffraction integrals in the paraxial (Eikonal) approximation. In the last step, this involved an incoherent sum over all coherent diffraction patterns associated with molecules starting from different source points, which caused limited spatial coherence, and with different velocities, which cause limited spectral coherence. To identify the contributing velocities we fit the molecular distribution on the screen to a Maxwell–Boltzmann velocity and took into account all vertical constraints in our set-up. We could thus assign the forward velocity of a molecule according to its vertical position on the screen. The van der Waals interaction between the polarizable molecule and the dielectric grating wall was taken into account in the phase of the grating transmission function. The phase term $\psi = \exp(iC_3D[1/\Delta x^3 + 1/(s-\Delta x)^3]/\hbar v)$ was multiplied by the binary transmission function given by the period and opening fraction of the grating. C_3 denotes the van der Waals constant, which we determined from a numerical fit of the expected diffraction curve to the observed interference pattern. The distance Δx of a particular molecule to its nearest grating bar as well as its longitudinal velocity v and the grating thickness D are important for the effective momentum kick during passage through the grating. We assumed Δx to be constant for each molecule during the transit time through the grating. We neglected all fringe effects, such as attraction outside the grating slit. To illustrate the high significance of surface–wall interactions even for a grating as thin as 10 nm and a molecular transit time of only 100 ps, we compared our experimental data with different theoretical assumptions in Supplementary Fig. S2.

Received 30 December 2011; accepted 16 February 2012; published online 25 March 2012

References

1. Jönsson, C. Elektroneninterferenzen an mehreren künstlich hergestellten Feinspalten. *Z. Phys.* **161,** 454–474 (1961).
2. Zeilinger, A., Gähler, R., Shull, C. G., Treimer, W. & Mampe, W. Single- and double-slit diffraction of neutrons. *Rev. Mod. Phys.* **60,** 1067–1073 (1988).
3. Keith, D. W., Schattenburg, M. L., Smith, H. I. & Pritchard, D. E. Diffraction of atoms by a transmission grating. *Phys. Rev. Lett.* **61,** 1580–1583 (1988).
4. Carnal, O. & Mlynek, J. Young's double-slit experiment with atoms: a simple atom interferometer. *Phys. Rev. Lett.* **66,** 2689–2692 (1991).
5. Schöllkopf, W. & Toennies, J. P. Nondestructive mass selection of small van der Waals clusters. *Science* **266,** 1345–1348 (1994).
6. Arndt, M. *et al.* Wave–particle duality of C_{60} molecules. *Nature* **401,** 680–682 (1999).
7. Zhao, B. S., Meijer, G. & Schollkopf, W. Quantum reflection of He_2 several nanometers above a grating surface. *Science* **331,** 892–894 (2011).
8. Crease, R. P. The most beautiful experiment in physics. *Phys. World* **15,** 15–17 (September 2002).
9. The double-slit experiment; available at http://physicsworld.com/cws/article/print/9745 (2002).
10. Merli, P., Missiroli, G. & Pozzi, G. On the statistical aspect of electron interference phenomena. *Am. J. Phys.* **44,** 306–307 (1976).
11. Tonomura, A., Endo, J., Matsuda, T., Kawasaki, T. & Ezawa, H. Demonstration of single-electron buildup of an interference pattern. *Am. J. Phys.* **57,** 117–120 (1989).
12. Feynman, R., Leighton, R. B. & Sands, M. L. in *Quantum Mechanics* Vol. 3, Ch. 1 (Addison Wesley, 1965).
13. Juffmann, T. *et al.* Wave and particle in molecular interference lithography. *Phys. Rev. Lett.* **103,** 263601 (2009).
14. Szriftgiser, P., Guéry-Odelin, D., Arndt, M. & Dalibard, J. Atomic wave diffraction and interference using temporal slits. *Phys. Rev. Lett.* **77,** 4–7 (1996).
15. Garcia, N., Saveliev, I. G. & Sharonov, M. Time-resolved diffraction and interference: Young's interference with photons of different energy as revealed by time resolution. *Phil. Trans. R. Soc. A* **360,** 1039–1059 (2002).
16. Lindner, F. *et al.* Attosecond double-slit experiment. *Phys. Rev. Lett.* **95,** 040401 (2005).
17. Akoury, D. *et al.* The simplest double slit: interference and entanglement in double photoionization of H_2. *Science* **318,** 949–952 (2007).
18. Canton, S. E. *et al.* Direct observation of Young's double-slit interferences in vibrationally resolved photoionization of diatomic molecules. *Proc. Natl Acad Sci. USA* **108,** 7302–7306 (2011).
19. Zimmermann, B. *et al.* Localization and loss of coherence in molecular double-slit experiments. *Nature Phys.* **4,** 649–655 (2008).
20. Nairz, O., Arndt, M. & Zeilinger, A. Quantum interference experiments with large molecules. *Am. J. Phys.* **71,** 319–325 (2003).
21. Born, M. & Wolf, E. *Principles of Optics* (Pergamon Press, 1993).
22. Wohlfart, K. *et al.* Alternating-gradient focusing and deceleration of large molecules. *Phys. Rev. A* **77,** 031404R (2008).
23. Deachapunya, S. *et al.* Slow beams of massive molecules. *Eur. Phys. J. D* **46,** 307–313 (2007).
24. Gerlich, S. *et al.* Quantum interference of large organic molecules. *Nature Commun.* **2,** 263 (2011).
25. Nairz, O., Arndt, M. & Zeilinger, A. Experimental challenges in fullerene interferometry. *J. Mod. Opt.* **47,** 2811–2821 (2000).
26. Compagnon, I., Antoine, R., Rayane, D., Broyer, M. & Dugourd, P. Vibration induced electric dipole in a weakly bound molecular complex. *Phys. Rev. Lett.* **89,** 253001 (2002).
27. Gring, M. *et al.* Influence of conformational molecular dynamics on matter wave interferometry. *Phys. Rev. A* **81,** 031604 (2010).
28. Moerner, W. E. & Kador, L. Optical detection and spectroscopy of single molecules in a solid. *Phys. Rev. Lett.* **62,** 2535–2538 (1989).
29. Hell, S. W. & Wichmann, J. Breaking the diffraction resolution limit by stimulated emission: stimulated-emission-depletion fluorescence microscopy. *Opt. Lett.* **19,** 780–782 (1994).
30. Gordon, M. P., Ha, T. & Selvin, P. R. Single-molecule high-resolution imaging with photobleaching. *Proc. Natl Acad. Sci. USA* **101,** 6462–6465 (2004).
31. Gerlich, S. *et al.* A Kapitza–Dirac–Talbot–Lau interferometer for highly polarizable molecules. *Nature Phys.* **3,** 711–715 (2007).
32. Grisenti, R. E., Schöllkopf, W., Toennies, J. P., Hegerfeldt, G. C. & Köhler, T. Determination of atom–surface van der Waals potentials from transmission-grating diffraction intensities. *Phys. Rev. Lett.* **83,** 1755–1758 (1999).
33. Juffmann, T. *et al.* Wave and particle in molecular interference lithography. *Phys. Rev. Lett.* **103,** 263601 (2009).
34. Nairz, O., Brezger, B., Arndt, M. & Zeilinger, A. Diffraction of complex molecules by structures made of light. *Phys. Rev. Lett.* **87,** 160401 (2001).
35. Juffmann, T., Nimmrichter, S., Arndt, M., Gleiter, H. & Hornberger, K. New prospects for de Broglie interferometry. *Found. Phys.* **42,** 98–110 (2010).
36. Hornberger, K., Gerlich, S., Haslinger, P., Nimmrichter, S. & Arndt, M. Quantum interference of clusters and molecules. *Rev. Mod. Phys.* **84,** 157–173 (2012).
37. Alzeer, J., Roth, P. J. C. & Luedtke, N. W. An efficient two-step synthesis of metal-free phthalocyanines using a Zn(II) template. *Chem. Commun.* 1970–1971 (2009).

Acknowledgements

This project was funded by the FWF (contract FWF-Z149-N16; Wittgenstein) and the ESF/FWF EuroCore Program MIME (I146). The authors thank P. Geyer and P. Haslinger for building the *in situ* sputter cleaning apparatus, S. Deachapunya for his collaboration in testing the vapour pressures of PcH2, S. Nimmrichter for theory support and M. Tomandl for rendering Fig. 1. M.A. thanks W.E. Moerner for helpful discussions on single-molecule fluorescence. The chemical synthesis in Basel was supported by the ESF EuroCore Programme MIME (I146-N16), the Swiss National Science Foundation, and the NCCR 'Nanoscale Science'.

Author contributions

T.J. and M.A. conceived the experiments. T.J., A.M., M.Mu. and O.C. worked on the set-up of the experiment. T.J. performed the diffraction experiments. J.T. and M.Ma. designed and synthesized the $F_{24}PcH_2$ molecules. A.T. and O.C. fabricated the 10 nm diffraction gratings. P.A. developed the basis for the micro-evaporation source. M.A. and T.J. wrote the paper, with comments by all authors.

Additional information

The authors declare no competing financial interests. Supplementary information accompanies this paper at www.nature.com/naturenanotechnology. Reprints and permission information is available online at http://www.nature.com/reprints. Correspondence and requests for materials should be addressed to M.A.